# Evaluation of an accelerogram-based liquefaction detection method using continuous earthquake recordings

Weiwei Zhan[1] & Qiushi Chen[2]
[1]*Department of Civil and Environmental Engineering, Tufts University, Medford, Massachusetts, USA*
[2]*The Glenn Department of Civil Engineering, Clemson University, Clemson, South Carolina, USA*


ABSTRACT
Accelerogram-based liquefaction detection methods directly use the earthquake records at the ground surface to assess liquefaction occurrence. We have recently developed a new accelerogram-based liquefaction detection method (Zhan and Chen 2021a) that uses two frequency-related ground motion parameters and the logistic regression algorithm to classify liquefaction occurrence. This method achieves an overall accuracy of over 90% when applied to a dataset consisting of 167 strong ground motions from seventeen worldwide earthquakes. In this study, we evaluate the performance of the new method using continuous earthquake recordings at four seismic stations. The results suggest the method performs better at the soft-soil sites than at the stiff-soil sites and tends to make false negative predictions for very strong earthquakes. This study highlights the applicability of the new accelerogram-based method to regions with continuous earthquake monitoring.

RÉSUMÉ
Les méthodes de détection de liquéfaction basées sur l'accélérogramme utilisent directement les enregistrements de tremblement de terre à la surface du sol pour évaluer l'occurrence de la liquéfaction. Nous avons récemment développé une nouvelle méthode de détection de liquéfaction basée sur un accélérogramme (Zhan et Chen 2021a) qui utilise deux paramètres de mouvement du sol liés à la fréquence et l'algorithme de régression logistique pour classer l'occurrence de la liquéfaction. Cette méthode atteint une précision globale de plus de 90 % lorsqu'elle est appliquée à un ensemble de données composé de 167 mouvements forts du sol provenant de dix-sept tremblements de terre dans le monde. Dans cette étude, nous évaluons les performances de la nouvelle méthode en utilisant des enregistrements continus de séismes à quatre stations sismiques. Les résultats suggèrent que la méthode fonctionne mieux sur les sites de sol mou que sur les sites de sol raide, et tend à faire de fausses prédictions négatives pour les tremblements de terre très forts. Cette étude met en évidence l'applicabilité de la nouvelle méthode basée sur l'accélérogramme aux régions bénéficiant d'une surveillance continue des tremblements de terre.

## 1. INTRODUCTION

Soil liquefaction is one type of earthquake-induced hazards that continually threatens the infrastructure safety. The most commonly used method for liquefaction triggering assessment is the simplified stress-based procedure that compares the seismic demand parameter (cyclic stress ratio, CSR) and the capacity parameter of the soil's resistance to liquefaction (cyclic resistance ratio, CRR) via deterministic or probabilistic manners (Youd et al. 2001; NASEM 2016). CSR is estimated using the peak ground acceleration in horizontal direction ($a_{max}$) and the empirical stress reduction coefficients along the depth ($r_d$). CRR is empirically correlated with the direct measures of in-field soil experiments such as the standard penetration test (SPT) (Seed and Idriss 1971), cone penetration test (CPT) (Robertson and Wride 1998), and shear-wave velocity measurements (Vs) (Andrus and Stokoe 2000). The simplified stress-based methods are widely used in both pre-earthquake design phase and post-earthquake hazard assessment. However, this type of methods are the expensive cost of in-field soil experiments and inaccurate estimations of earthquake loading parameters (e.g., $a_{max}$ and $r_d$).

Accelerogram-based liquefaction detection methods directly use the earthquake records (i.e., accelerograms) at the ground surface to assess liquefaction occurrence. Intrinsically, the accelerogram-based methods assess the liquefaction occurrence based on the liquefaction effects on the accelerograms. In other words, they learn the differences between liquefaction-affected accelerograms and other accelerograms. Existing accelerogram-based methods are mostly for the deterministic evaluation of the liquefaction occurrence (Suzuki et al. 1998; Miyajima 1998; Ozaki 1999; Kostadinov and Yamazaki 2001; Yuan et al. 2010), and one recent study has been developed to assess the liquefaction initiation time (Özener et al. 2020). The existing accelerogram-based liquefaction detection methods usually include two components. The first component is to extract ground motion parameters capable of representing liquefaction effects on the accelerograms (e.g., changes of site natural period due to the soil softening effects of liquefaction). This parameter extraction process can utilize different signal processing techniques

(e.g., integration of acceleration time histories, Fourier transform, short-time Fourier transform). Kostadinov and Yamazaki (2001) found that frequency-related ground motion parameters are the most effective parameters for the accelerogram-based liquefaction detection method when compared with the amplitude- and energy-related ground motion parameters. The second component of the liquefaction-detection methods is to decide the classification criteria to separate liquefaction-affected accelerograms and other accelerograms, which usually use some threshold values of the extracted ground motion parameters. These threshold values are usually determined from accelerogram datasets of several earthquakes and need recalibration for applications to different earthquakes (Miyajima 1998). As these two components are computationally cheap, the accelerogram-based liquefaction detection methods can be applied in real-time liquefaction hazard mitigation for regions with dense seismic monitoring networks, such as the Tokyo urban area (Shimizu et al. 2000). Besides, we want to claim that the accelerogram-based liquefaction detection methods can also be used to select more liquefaction-affected ground motions from the existing seismic waveform database to advance the response spectra study at liquefaction sites (e.g., Gingery et al. 2016).

In Zhan and Chen (2021a), we present a new accelerogram-based method that can probabilistically assess the liquefaction occurrence using an expanded global dataset. The framework of the development process of the new accelerogram-based liquefaction detection method consists of four main steps (Figure 1). Step 1 is to extract ground motion parameters (features) from the two horizontal accelerograms that can well separate liquefaction-affected accelerograms and other accelerograms. We used two frequency-related ground motion parameters that can be directly extracted from any accelerogram. The first parameter is called the ratio of the low-frequency portion to the whole area of the Fourier amplitude spectrum (termed RL), the upper frequency limits for the low-frequency portion and the whole Fourier amplitude spectrum are set as 1 Hz and 10 Hz, respectively. RL is an indicator of the relative richness of the low-frequency components in a ground motion record. The second parameter is called the mean instantaneous frequency decrease rate (termed MIFr), that describes the change rate of the mean instantaneous frequency within the 10 sec window after the PGA time and the mean instantaneous frequency within the 10 sec window before the PGA time. MIFr indicates the temporal variation rate of the mean instantaneous frequency. The RL and MIFr can be extracted using the Fourier transform (FT) and short-time Fourier transform (STFT) following Zhan and Chen (2021a). Step 2 is to compile a database that consisted of 132 case histories with both liquefaction observations (yes or no) and earthquake recordings. Step 3 is to build a logistic regression model to classify liquefaction or non-liquefaction given the RL and MIFr as the explanatory variables. The output of the Step 3 is originally a probability indicator of liquefaction occurrence (termed LQI). Based on the database compiled in Step 2, we recommend a LQI threshold of 0.15 for the binary classification of liquefaction occurrence. Step 4 is to validate the model performance using an independent dataset consisting of 32 case histories from the 2001 Mw 6.8 Nisqually earthquake and compare the model performance with existing accelerogram-based liquefaction detection methods. Our new accelerogram-based liquefaction detection method shows plausible accuracies and promising potentials for applications in real-time liquefaction hazard mitigation systems. One of our follow-up studies has investigated the sensitivity of the two ground motion frequency parameters (RL and MIFr) used in the new accelerogram-based liquefaction detection method to different earthquake source, path, and site factors (Zhan and Chen 2021b). The sensitivity analyses results suggest that soil liquefaction generally has a dominant effect on the two ground motion frequency parameters, which supports that accelerograms only can be used to separate liquefaction and non-liquefaction. However, the sensitivity studies also suggest that the earthquake magnitude (earthquake source effects) can affect the MIFr and the epicentral distance can affect the RL (path effects) to similar level of liquefaction effects.

The model development and validation (Zhan and Chen 2021a) and the sensitivity (Zhan and Chen 2021b) studies used a dataset consisting of 167 strong ground motions from seventeen worldwide earthquakes (Zhan and Chen 2021a). This dataset is representative for evaluating the model effectiveness across different sites. This work aims to evaluate the effectiveness of the new accelerogram-based liquefaction detection method across different earthquakes. To achieve this goal, we selected four seismic stations with decade-long earthquake recordings.

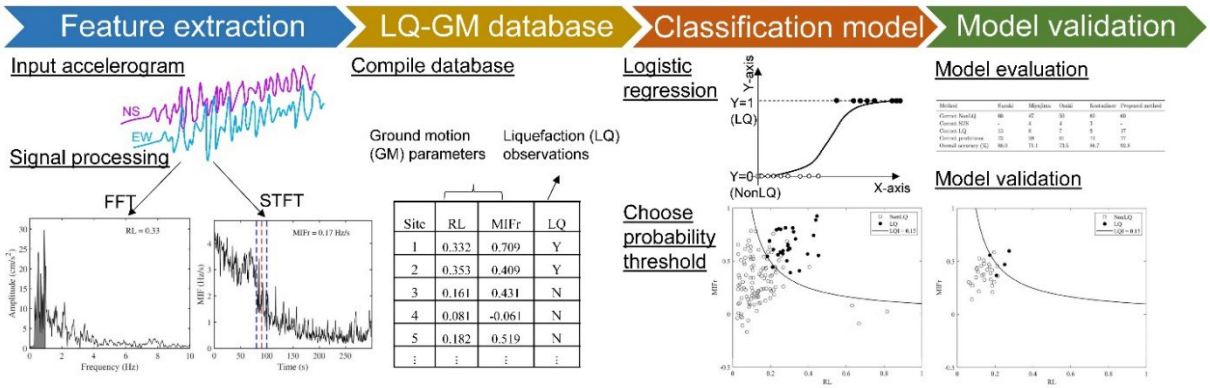


Figure 1. Framework of the accelerogram-based liquefaction detection method developed by Zhan and Chen (2021a)

## 2. DATA AND METHODS

### 2.1 Accelerogram-based liquefaction detection method

The procedure of the new accelerogram-based liquefaction detection method (Zhan and Chen 2021a) is shown in Figure 2, and an automated implementation code of the procedure is available the Github repository: https://github.com/qschen/liquefaction-detection.git. The procedure starts with two horizontal accelerograms as inputs, which are obtainable from most seismic stations. We then filter out low-intensity ground motions that are not likely going to trigger liquefaction but may affect the RL and MIFr computations due to large components of noise. We use the peak ground acceleration (PGA) of 78 cm/s$^2$ (0.08g) based on a recent study about the minimum peak ground acceleration to trigger liquefaction (de Magistris et al. 2013). Then, we compute RL and MIFr for each horizontal accelerogram and then take their arithmetic mean value as the corresponding values for the station. The details of the signal processing are available in Zhan and Chen (2021a). Finally, we compute the liquefaction indicator (LQI) using the logistic regression model (Equation 1) and use the LQI threshold of 0.15 to classify the liquefaction occurrence.

$$\mathrm{LQI} = \frac{1}{1 + e^{6.44 - 47.61 \times \mathrm{RL} \times \mathrm{MIFr}}} \quad [1]$$

where LQI is the liquefaction indicator, and its value is between 0 and 1 with larger values indicating higher probability of liquefaction; RL is the ratio of low-frequency portion to the total area of the Fourier amplitude spectrum; and MIFr is the mean instantaneous frequency decrease rate.

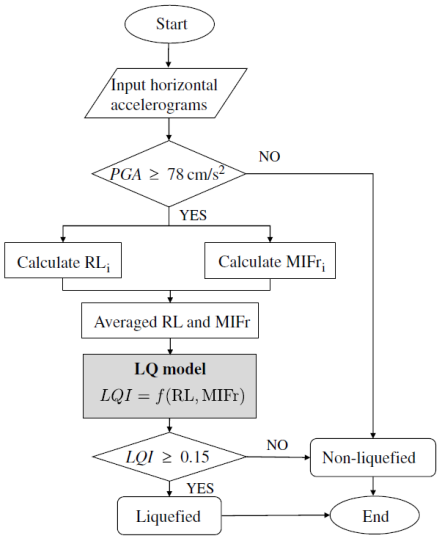


Figure 2. Procedure of the accelerogram-based liquefaction detection method (from Zhan and Chen 2021a).

### 2.2 Ground motion data and liquefaction labeling

To test the performance of the new accelerogram-based liquefaction detection method at a single site across different earthquakes, we selected four seismic stations that have decade-long earthquake recordings and reported liquefaction evidence from at least one earthquake. These four stations are the Wildlife Liquefaction Array (WLA) in the United States, the Port Island Array (PIA), the Kushiro Port Array (KPA), and the Onahama Port Array (OPA) in Japan. The WLA and PIA have the time-averaged shear-wave velocity to 30 m depth (Vs30) of 177 m/s and 199 m/s. The KPA has Vs30 of 321 m/s and the OPA has Vs11 (the time-averaged shear-wave velocity to 11 m depth) of 493 m/3 according to available soil profile data. In total, we collected all available earthquake recordings recorded between the instrumentation date and May 2020 at each station, and the total number of earthquakes is 520, 189, 199, and 1238 at the WLA, PIA, KPA, and OPA stations, respectively. The summary statistics and location information of these earthquakes are available in Zhan and Chen (2022). The accelerograms at three Japanese sites were downloaded from the Japanese Port and Airport Research Institute (PARI) seismic network (website https://www.pari.go.jp/), and those at the WLA were downloaded from the Network for Earthquake Engineering Simulation at University of California, Santa Barbara (NEES@UCSB) (http://nees.ucsb.edu/facilities/wla).

To evaluate the effectiveness of the new accelerogram-based liquefaction detection method at the four stations, we first filter out low-intensity ground motion records (i.e., with PGA at the ground surface less than 0.08 g). Adding these low-intensity ground motions into the model evaluation could only increase the model accuracies because it will increase the number of correct non-liquefaction predictions. The number of filter-out strong ground motions, and the magnitude (Mw) and epicentral distance (Repi) of their source earthquakes are summarized in Table 2. Generally, these strong ground motions are induced by earthquakes with magnitude ranging from M 2.8 to 9.0, and have Repi of 4 to 272 km and PGA of 0.08 to 1.83 g.

We then need to label the ground-truth of liquefaction occurrence for each strong ground motions and each site. We label the ground motions as liquefaction-triggering ground motions if there is a reported evidence of soil liquefaction in the literature. Otherwise, the ground motions will be labelled as non-liquefaction-triggering ground motions. Following these criteria, we label six ground motions as liquefaction-triggering ground motions, including the 1987 Mw 6.6 Superstition Hills earthquake at the WLA, the 1995 M 7.3 Hyogoken-Nanbu earthquake at the PIA, the 1993 M 7.6 Kushiro-Oki, 1994 M 8.2 Hokkaido Toho-Oki, 2003 M 8.0 Tokachi-Oki earthquakes at the KPA, and the 2011 M 9.0 Tohoku earthquake at the OPA. Liquefaction evidence of these six liquefaction-triggering ground motions is detailed in Zhan and Chen (2022). It is noted that the labeling process involve uncertainty

because: 1) some liquefaction-triggering ground motions may not have been reported in the literature; 2) the quality of liquefaction evidence reported in the literature may vary from site to site and from earthquake to earthquake. For example, the liquefaction-triggering ground motions at the WLA, PIA, OPA are of high certainty as sand boils were observed at the three sites according to the field survey (Holzer et al. 1989; Yamazaki et al. 1995; Kramer et al. 2016). The liquefaction evidence at KPA was indirect evidence, such as cyclic mobility acceleration spikes within the accelerograms (Kostadinov and Yamazaki 2001) and shear wave velocity reduction from the inverse analysis (Thabet et al. 2008). The effects of liquefaction labeling uncertainties will be discussed in the "RESULTS" section.

Table 1. Summary of the strong ground motion data at the four seismic stations.

| Station | *Nstr* | *Nliq* | *emag* (M) | *Repi* (km) | PGA (g) |
|---|---|---|---|---|---|
| WLA | 17 | 1 | 3.3~6.6 | 7~15 | 0.09~0.31 |
| PIA | 5 | 1 | 2.8~7.3 | 4~45 | 0.08~0.43 |
| KPA | 12 | 3 | 5.1~8.2 | 9~272 | 0.09~0.59 |
| OPA | 26 | 1 | 3.1~9.0 | 9~215 | 0.08~1.83 |

Note: *Nstr* is the number of strong ground motions (with surface PGA>=0.08g); *Nliq* is the number of liquefaction-triggering strong ground motions; *emag* is the earthquake magnitude; and *Repi* is the epicentral distance to the station.

## 3. RESULTS

We use multiple classification performance metrics to evaluate the performance of the new accelerogram-based liquefaction detection method at the four stations across different earthquakes. There are four possible prediction outcomes of the classification model for each earthquake recorded at each site, namely, true positive (TP, i.e., liquefaction is predicted and observed), false positive (FP, i.e., liquefaction is predicted but not observed), true negative (TN, i.e., liquefaction is not predicted and not observed), and false negative (FN, i.e., liquefaction is not predicted but is observed). We use *precision*, *recall*, *accuracy*, and *f1 score* to evaluate the model performance. The *precision* (also called the true positive rate) describes how many positive predictions are actually correct and is computed following Equation 2. The *recall* describes how good the model correctly predicts all the positive observations and is computed using Equation 3. The *accuracy* describes the ratio of the number of correct predictions and the total number of predictions and is computed following Equation 4. The *f1 score* is the harmonic mean of *precision* and *recall* (see Equation 5). The classification performance metrics of the accelerogram-based liquefaction detection method at the four stations are summarized in Table 2. The classification chart for earthquakes at each station are visualized in Figure 3 (in which the black curves indicate the decision boundary with threshold LQI of 0.15).

$$precision = \frac{TP}{TP+FP} \quad [2]$$

$$recall = \frac{TP}{TP+FN} \quad [3]$$

$$accuracy = \frac{TP+TN}{TP+FN+TN+FP} \quad [4]$$

$$f1\ score = \frac{2 \times precision \times recall}{precision + recall} \quad [5]$$

where TP, FP, TN, and FN are the number of true positive, false positive, true negative, and false negative predictions.

Table 2. Classification performance for the four selected stations.

| Station | *precision* (%) | *recall* (%) | *accuracy* (%) | *f1 score* (%) |
|---|---|---|---|---|
| WLA | 100 | 100 | 100 | 100 |
| PIA | 100 | 100 | 100 | 100 |
| KPA | 100 | 33.3 | 83.33 | 50 |
| OPA | 0 | 0 | 96.15 | 0 |

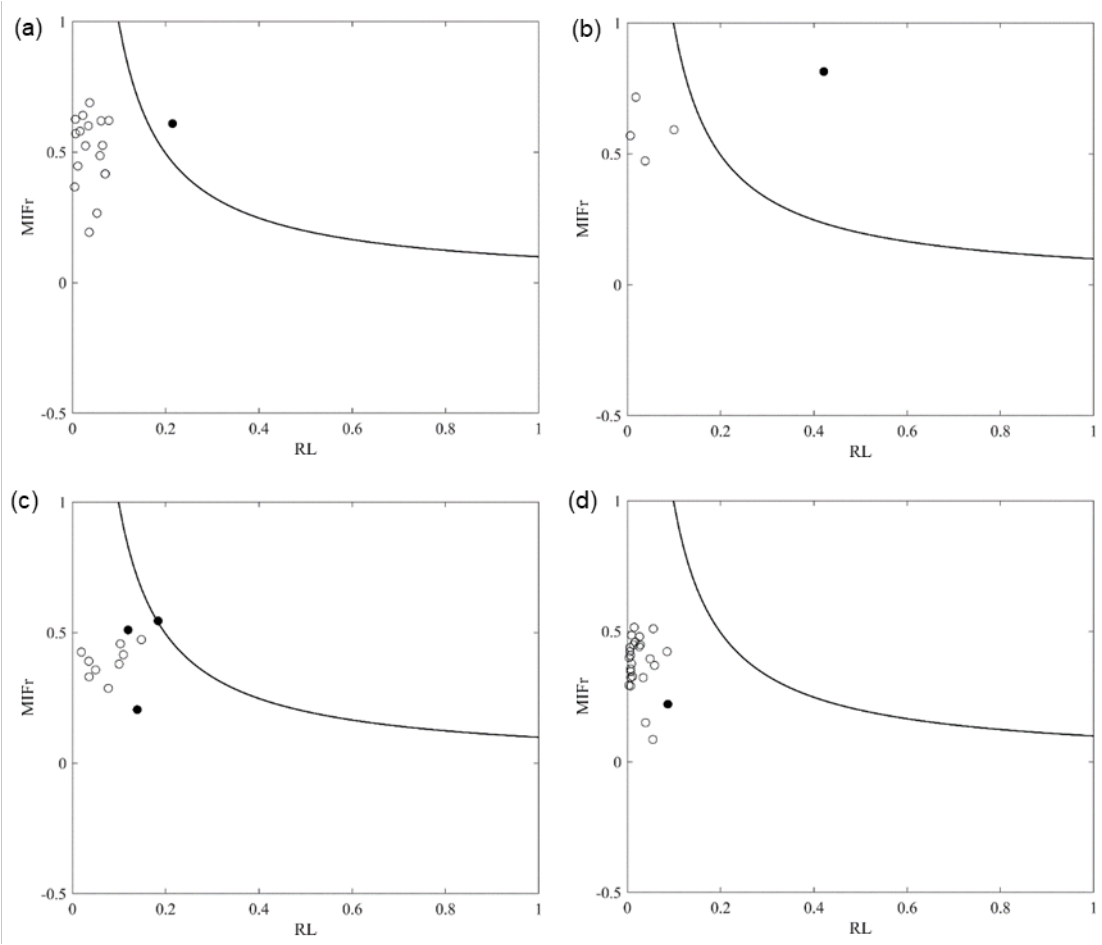


Figure 3. Evaluation results of the accelerogram-based liquefaction detection method across multiple earthquakes at the: (a) Wildlife Liquefaction Array (WLA); (b) Port Island Array (PIA); (c) Kushiro Port Array (KPA); and (d) Onahama Port Array (OPA). The solid and empty circles indicate ground motions did and did not triggered liquefaction, respectively.

According to Figure 3, our new accelerogram-based liquefaction detection method has no false positive predictions at the four stations. The new accelerogram-based method performs better at the two soft-soil sites (WLA and PIA) than at the two stiff-soil sites (KPA and OPA). At the WLA and PIA stations, the liquefaction-triggering ground motions are well separated from the non-liquefaction-triggering ground motions (Figures 3a and 3b). The *precision*, *recall*, *accuracy*, and *f1 score* are 100% at the WLA and PIA. As for the KPA station, the new accelerogram-based method has two false negative predictions that are associated with the 1994 M 8.2 Hokkaido Toho-Oki earthquake and the 2003 M 8.0 Tokachi-Oki earthquake (Figure 5). As the MIFr of the 2003 earthquake recordings shows unexpected low values, we visualize the MIFr computation process of the 2003 earthquake along with that of the 1993 earthquake (true positive prediction) in Figure 4. Figure 7 shows that the time window of MIFr computation for the TP earthquake appears about 10 sec later than that for the FN earthquake, which adversely affects the MIFr computation. We suggest future studies can use the seismic phase information instead of the PGA time to determine the time window for MIFr computation. Besides, the two false negative predictions at the KPA may be caused by the uncertain liquefaction observations of these two earthquakes. Thabet et al. (2008) suggested these two earthquakes triggered liquefaction based on their inverse analysis of shear wave velocity reductions. As there is no surface manifestation of liquefaction occurrence at KPA under these two earthquakes, the liquefaction may be mislabeled. The false negative prediction at the OPA is associated with the 2011 M 9.0 Tohoku earthquake (Figure 3d). As the TP becomes zero at the OPA, the precision, recall, F1 score become to zeros (Table 2). The misprediction for the 2011 Tohoku earthquake may be caused by the complex fault rupture process of the 2011 Tohoku earthquake (involving at least three significant events according to Goto et al. 2013) that can adversely affect the MIFr computation with multiple MIF peaks (Figure 5).

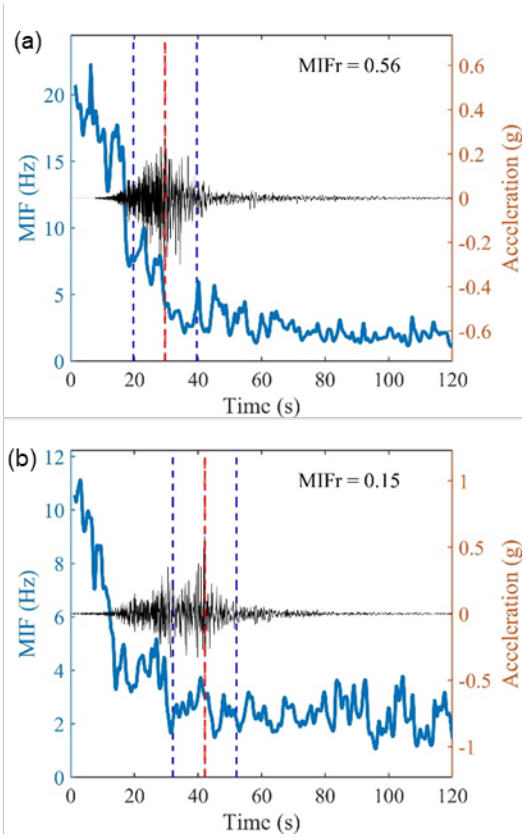


Figure 4. Time histories of the mean instantaneous frequency (MIF) and acceleration at the KPA for: (a) the north-south component of the 1993 M 7.6 Kushiro-Oki earthquake recordings (true positive prediction), and (b) the north-south component of the 2003 M 8.0 Tokachi-Oki earthquake recordings (false negative prediction). Note the blue dashed lines indicate the time window for the MIFr computation, and the red dashed line indicates the PGA time.

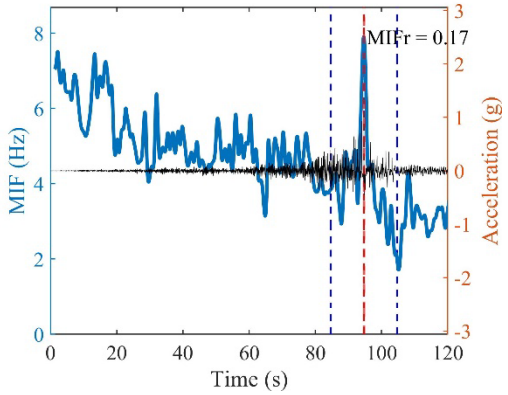


Figure 5. Time histories of the mean instantaneous frequency (MIFr) and acceleration for the north-south component of 2011 M 9.0 Tohoku earthquake recordings at the KPA.

## 4. CONCLUSION

In this work, we evaluate the performance of the new accelerogram-based liquefaction detection method developed by Zhan and Chen (2021a) using continuous earthquake recordings at four seismic stations. The results suggest that the accelerogram-based method has produced zero false positive predictions but three false negative predictions. The new accelerogram-based method shows higher accuracies at the two soft-soil sites (WLA and PIA) than at the two stiff-soil sites (KPA and OPA). The three false negative predictions are associated with the great earthquakes (with magnitude ≥ 8.0) that may involve complex fault process that affects the temporal change of the mean instantaneous frequency. Future studies will need to collect more real-world earthquake recordings and/or synthetic data to improve the model applicability to very strong earthquakes.

## REFERENCES

Andrus, R. D., and Stokoe II, K. H. 2000. Liquefaction resistance of soils from shear-wave velocity. *Journal of geotechnical and geoenvironmental engineering*, 126(11): 1015-1025.

de Magistris, F. S., Lanzano, G., Forte, G., and Fabbrocino, G. 2013. A database for PGA threshold in liquefaction occurrence. *Soil Dynamics and Earthquake Engineering*, 54, 17-19.

Gingery, J. R., Elgamal, A., and Bray, J. D. 2015. Response spectra at liquefaction sites during shallow crustal earthquakes. *Earthquake Spectra*, 31(4), 2325–2349.

Goto, H., Hata, Y., Kuwata, Y., Yamamoto, H., Morikawa H., and Kataoka, S. 2013. Earthquake source and ground motion characteristics in eastern Japan during the 2011 off the Pacific Coast of Tohoku earthquake. *Journal of JSCE*, 1(1):329~342.

Kostadinov, M. V. and Yamazaki, F. 2001. Detection of soil liquefaction from strong motion records. *Earthquake Engineering and Structural Dynamics*, 30(2), 173–193.

Kramer, S. L., Asl, B. A., Ozener, P., and Sideras, S. S. 2015. Effects of liquefaction on ground surface motions." *Perspectives on Earthquake Geotechnical Engineering*, Springer, 285–309.

Miyajima, M. 1998. Detective method of liquefaction using strong ground motion records. *Proceedings of the 3rd China-Japan-US Trilateral Symposium on Lifeline Earthquake Engineering*, Kunming, China, August 1998,133–140. Beijing: China Earthquake Administration.

Ozaki, R. 1999. Study on real-time earthquake mitigation liquefaction monitoring and earthquake countermeasures. PhD Thesis, Kobe University.

Özener, P. T., Greenfield, M. W., Sideras, S. S., and Kramer, S. L. 2020. Identification of time of liquefaction triggering. *Soil Dynamics and Earthquake Engineering*, 128, 105895.

Robertson, P. K., and Wride, C. E. 1998. Evaluating cyclic liquefaction potential using the cone penetration test. *Canadian geotechnical journal*, 35(3): 442-459.

Seed, H. B., and Idriss, I. M. 1971. Simplified procedure for evaluating soil liquefaction potential. *Journal of the Soil Mechanics and Foundations division*, 97(9): 1249-1273.

Shimizu, Y., Watanabe, A., Koganemaru, K., Nakayama, W., and Yamazaki, F. 2000. Super high-density realtime disaster mitigation system. *12th World Conference on Earthquake Engineering*, Vol. 7.

Suzuki, T., Shimizu, Y., and Nakayama, W. 1998. Characteristics of strong motion records at the liquefied sites and judgment for liquefaction. *11th European Conference on Earthquake Engineering*. Rotterdam, Netherlands: A.A. Balkema.

Thabet, M., Nemoto, H., and Nakagawa, K. 2008. Variation process in stiffness inferred by nonlinear inversion during mainshocks at Kushiro Port vertical array site. *Earth, planets and space*, 60(6):581–589.

Youd, T. L., et al. 2001. Liquefaction resistance of soils: Summary report from the 1996 NCEER and 1998 NCEER/NSF workshops on evaluation of liquefaction resistance of soils." *Journal of Geotechnical and Geoenvironmental Engineering,* 127 (10): 817–833.

Yuan, X., Sun, R., Chen, L., and Tang, F. 2010. A method for detecting site liquefaction by seismic records. *Soil Dynamics and Earthquake Engineering*, 30(4): 270-279.

Zhan, W., and Chen, Q. 2021a. Accelerogram-Based Method for Quick Assessment of Liquefaction Occurrence. *Journal of Geotechnical and Geoenvironmental Engineering*, 147(8), 04021060.

Zhan, W., and Chen, Q. 2021b. Assessment of Liquefaction Effects on Ground Motion Frequency Parameters for Accelerogram-Based Liquefaction Detection. *ASCE Geo-Extreme 2021*, Savannah, Georgia, USA: 318-327.

Zhan, W., and Chen, Q. 2022. Nonlinear site response at liquefiable sites: Insights from downhole seismic observations. *Engineering Geology*, 301, 106610.